CHALMERS
UNIVERSITY OF TECHNOLOGY

# Numerical homogenization of spatial network models

Downloaded from: https://research.chalmers.se, 2024-04-17 14:44 UTC

Citation for the original published paper (version of record):
Edelvik, F., Görtz, M., Hellman, F. et al (2024). Numerical homogenization of spatial network models. Computer Methods in Applied Mechanics and Engineering, 418.
http://dx.doi.org/10.1016/j.cma.2023.116593

N.B. When citing this work, cite the original published paper.

research.chalmers.se offers the possibility of retrieving research publications produced at Chalmers University of Technology.
It covers all kind of research output: articles, dissertations, conference papers, reports etc. since 2004.
research.chalmers.se is administrated and maintained by Chalmers Library

(article starts on next page)

Computer Methods in Applied Mechanics and Engineering 418 (2024) 116593

Contents lists available at ScienceDirect

Comput. Methods Appl. Mech. Engrg.

journal homepage: www.elsevier.com/locate/cma

# Numerical homogenization of spatial network models

F. Edelvik [a], M. Görtz [a,b,*], F. Hellman [b], G. Kettil [a], A. Målqvist [b]

[a] Computational Engineering and Design, Fraunhofer-Chalmers Centre, Chalmers Science Park, Gothenburg, 412 88, Sweden
[b] Department of Mathematical Sciences, Chalmers University of Technology and University of Gothenburg, Gothenburg, 412 96, Sweden

ARTICLE INFO

*Keywords:*
Algebraic connectivity
Discrete model
Multiscale method
Network model
Localized orthogonal decomposition
Upscaling

ABSTRACT

We present and analyze a methodology for numerical homogenization of spatial networks models, e.g. heat conduction and linear deformation in large networks of slender objects, such as paper fibers. The aim is to construct a coarse model of the problem that maintains high accuracy also on the micro-scale. By solving decoupled problems on local subgraphs we construct a low dimensional subspace of the solution space with good approximation properties. The coarse model of the network is expressed by a Galerkin formulation and can be used to perform simulations with different source and boundary data, at a low computational cost. We prove optimal convergence to the micro-scale solution of the proposed method under mild assumptions on the homogeneity, connectivity, and locality of the network on the coarse scale. The theoretical findings are numerically confirmed for both scalar-valued (heat conduction) and vector-valued (linear deformation) models.

## 1. Introduction

In order to reduce complexity in computer simulation, first principle models on materials composed of multiple slender domains are sometimes replaced by simpler spatial network models. In a porous media flow problem, for instance, continuum-scale fluid flow equations in the three-dimensional pore space geometry can be replaced by a spatial network model where the nodes represent pore cavities and the edges model throats between cavities, see e.g. [1]. Another example is deformation of fiber based materials, like paper and cardboard, where individual fibers can be modeled as one-dimensional objects instead of three-dimensional hollow cylinders, resulting in a spatial network model of edges (fibers) and nodes (connections between fibers), see [2]. Still, the resulting network models are often very large and the edge weights (modeling e.g. permeability or fiber width) may vary rapidly in space. See Fig. 1 for an illustration and [3] for more details on a paper model. The aim of this work is to develop and analyze a numerical homogenization technique for spatial network models that maintains high accuracy on the micro-scale.

Problems where the micro-scale model is a partial differential equation (PDE) instead of a spatial network model are well-studied in the literature. Homogenization theory efficiently handles numerical upscaling when the data variation is periodic. For non-periodic data, there are various numerical approaches. Successful numerical algorithms typically use parallelization and discretizations on multiple scales, for instance geometric multigrid [4] and domain decomposition [5] but also numerical homogenization techniques such as the multiscale finite element method [6], gamblets [7], and localized orthogonal decomposition (LOD) method [8,9]. It is natural to define coarser scales in PDE problems, at least if the geometry is simple, using nested meshes. In this work, we want to apply numerical homogenization techniques inspired by the PDE community to spatial network models, where it is less obvious how coarse scales can be introduced.

* Corresponding author.
*E-mail address:* morgan.gortz@fcc.chalmers.se (M. Görtz).

https://doi.org/10.1016/j.cma.2023.116593
Received 7 June 2023; Received in revised form 2 October 2023; Accepted 3 November 2023
Available online 9 November 2023
0045-7825/© 2023 The Authors. Published by Elsevier B.V. This is an open access article under the CC BY license (http://creativecommons.org/licenses/by/4.0/).

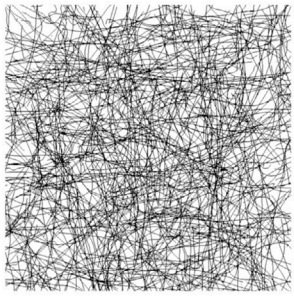

**Fig. 1.** A network model resulting from a paper forming simulation.

Numerical homogenization techniques from the PDE community have been applied to spatial network models before. In [10,11] the heat conductivity of a spatial network is studied. In these works, local solutions enable the construction of an effective global thermal conductivity tensor. Another approach is stochastic volume elements [12–14], where in [14], a network model was used to analyze the microstructure for the elements in the method. Traffic flows models in [15] consider a governing PDE for the macroscale by formulating traffic flow equations for single network nodes by interpreting the relations as finite difference approximations. The macroscale parameters are computed using a two-scale averaging technique. In [1] spatial network models of flows in a porous medium are studied. The network nodes represent pores and the edges represent throats. The micro-scale model is based on mass conservation equations for the flow through the network.

This paper considers the LOD method, which aims to produce accurate approximations on the micro-scale solution to the problem by constructing a representative low-dimensional function space. In [2], we consider a specific linear fiber deformation network model of paper and derive the LOD-based numerical method considered here. However, the key results needed to prove the convergence of the proposed method were left as open problems. In this paper, we take advantage of the recent work [16] on domain decomposition methods for spatial network models to prove optimal order convergence of the LOD method when applied to spatial network models.

We consider a spatial network, defined by a symmetric network matrix $\mathbf{K}$, for which we want to solve an equation of the form: find $\mathbf{u} \in \mathbf{V}$ such that for all $\mathbf{v} \in \mathbf{V}$,

$$(\mathbf{Ku}, \mathbf{v}) = (\mathbf{f}, \mathbf{v}),$$

given right hand side data $\mathbf{f}$ and with $(\cdot, \cdot)$ denoting the Euclidean scalar product taken over the nodes of the network. We apply the LOD method and introduce an artificial coarse-scale using minimal assumptions on the relation between the coarse-scale representation and the network. The fine-scale space is defined as the kernel of a projective quasi-interpolation operator onto the coarse-scale, and the multiscale space is the orthogonal complement to the fine-scale space with respect to the inner product induced by $\mathbf{K}$. In order to show optimal order convergence, we need to show that the basis spanning the multiscale space decays in space. This decay is possible to establish under mild assumptions on the homogeneity, connectivity, and locality of the network. In order to analyze the error in the proposed method, we prove an interpolation error bound in the spatial network setting. The theoretical findings show how the density variation and connectivity of the network affect the approximation properties of the proposed method. The main result is an optimal order a priori error bound in the norm induced by $\mathbf{K}$. Finally, the theoretical results are illustrated by three numerical examples.

The paper is organized as follows. Section 2 is devoted to preliminary notation and problem formulation. Section 3 introduces coarse finite element spaces and proves an interpolation error bound. In Section 4, the LOD method is presented and an a priori error bound is derived. Finally, in Section 5 numerical examples are presented. To get a better overview, some of the more technical proofs are presented in the Appendix.

## 2. Problem formulation

This section presents network notation, function spaces, norms, and finally the model problem, with three examples of network matrices $\mathbf{K}$ we consider.

### 2.1. Network and norms

We consider spatial networks represented as connected graphs $\mathcal{G} = (\mathcal{N}, \mathcal{E})$, where the node set $\mathcal{N}$ is a finite set of points $x \in \mathbb{R}^d$ and the edge set

$$\mathcal{E} = \{\{x, y\} \ : \ \text{an edge connects } x \text{ and } y\}$$

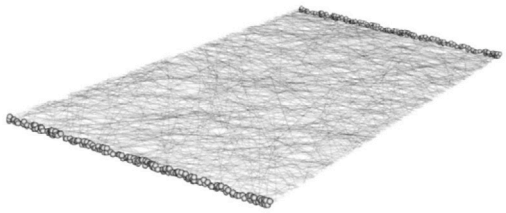

**Fig. 2.** A spatial network with Dirichlet nodes marked on opposite boundary segments.

consists of unordered node pairs. The notation $x \sim y$ means that $\{x, y\}$ is an edge in $\mathcal{E}$, i.e. $x$ and $y$ are adjacent. For simplicity we assume that the network resides in the hyper-rectangle

$$\Omega = [0, l_1] \times [0, l_2] \times \cdots \times [0, l_d],$$

however, the methodology can be generalized to polygonal and polyhedral domains. For each pair of adjacent nodes $x \sim y$ we write the Euclidean distance between the nodes as $|x - y|$. Furthermore, we let $\Gamma \subset \partial\Omega$ be the non-empty boundary segment where Dirichlet boundary conditions are applied. See Fig. 2 for an illustration.

Let the function space $\hat{V}$ be the space of real valued functions that are defined on the node set $\mathcal{N}$, and introduce the constrained space

$$V = \{v \in \hat{V} \ : \ v(x) = 0, x \in \Gamma\}.$$

In order to refer to a subset of nodes in the network we define $\mathcal{N}(\omega) = \mathcal{N} \cap \omega$ for any $\omega \subset \Omega$. Using this notation, let $(u, v)_\omega = \sum_{x \in \mathcal{N}(\omega)} u(x) \cdot v(x)$ and $(u, v) = (u, v)_\Omega$, for all $u, v \in \hat{V}$.

We further introduce a weighted version of the inner product. This weighted inner product is composed of node-wise diagonal linear operators $M_x : \hat{V} \to \hat{V}$:

$$(M_x v, v) = \frac{1}{2} \sum_{y \sim x} |x - y| v(x)^2. \tag{1}$$

These node-wise operators are extended to sets, $\omega \subset \Omega$, by $M_\omega = \sum_{x \in \mathcal{N}(\omega)} M_x$, with $M = M_\Omega$ when the full domain is considered. The weighted inner product

$$(Mu, v) = \sum_{x \in \mathcal{N}} (M_x u, v)$$

defines the norm

$$|v|_M = (Mv, v)^{1/2}$$

and, similarly, $|v|_{M,\omega} = (M_\omega v, v)^{1/2}$ the semi-norms. The squared norm $|1|^2_{M,\omega}$ of the constant function $1 \in \hat{V}$ can be interpreted as the mass of the network in subdomain $\omega$.

Next, we define semi-norms related to the reciprocal edge-length weighted graph Laplacian. Let

$$|v|^2_{L,\omega} = \frac{1}{2} \sum_{x \in \omega} \sum_{y \sim x} \frac{(v(x) - v(y))^2}{|x - y|}. \tag{2}$$

and, with a simplified notation,

$$|v|_L = |v|_{L,\Omega}.$$

We note that $|1|_L = 0$, since the weighted graph Laplacian has the constant functions of $\hat{V}$ in its kernel. However, since $1 \notin V$ and $\mathcal{G}$ is connected, $|\cdot|_L$ is a norm on $V$.

### 2.2. Vector-valued functions

The models considered in this work are both scalar-valued (e.g. heat conduction) and vector-valued (e.g. structural problems), so we need to introduce vector-valued function spaces and network operators. Let the integer $n$ denote the number of components in the function space of interest. We introduce

$$\mathbf{V} = V^n = V \times \cdots \times V$$

as the admissible function space for the unknown and $\hat{\mathbf{V}} = \hat{V}^n$ (so that $\mathbf{V} \subset \hat{\mathbf{V}}$) as the full space. In general, the different components (dimensions) of $\mathbf{V}$ can have separate Dirichlet boundary conditions, however, we assume, for simplicity, that all components are the same. A function $\mathbf{v} \in \hat{\mathbf{V}}$ consists of the components $v_1, v_2, \ldots, v_n$ and we write $\mathbf{v} = [v_1, v_2, \ldots, v_n]$.

We also introduce corresponding norms

$$|\mathbf{v}|_{\mathbf{L}} = \left( \sum_{i=1}^{n} |v_i|_L^2 \right)^{1/2}, \tag{3}$$

$$|\mathbf{v}|_{\mathbf{M}} = \left( \sum_{i=1}^{n} |v_i|_M^2 \right)^{1/2}, \tag{4}$$

with localized versions $|\mathbf{v}|_{\mathbf{L},\omega} = \left( \sum_{i=1}^{n} |v_i|_{L,\omega}^2 \right)^{1/2}$ and $|\mathbf{v}|_{\mathbf{M},\omega} = \left( \sum_{i=1}^{n} |v_i|_{M,\omega}^2 \right)^{1/2}$.

### 2.3. Model problem

The model problem is expressed using a linear operator $\mathbf{K} : \hat{\mathbf{V}} \to \hat{\mathbf{V}}$ and a function $\mathbf{f} \in \hat{\mathbf{V}}$:

$$\text{find } \mathbf{u} \in \mathbf{V} \ : \ (\mathbf{K}\mathbf{u}, \mathbf{v}) = (\mathbf{f}, \mathbf{v}) \text{ for all } \mathbf{v} \in \mathbf{V}. \tag{5}$$

Since $\mathbf{u} \in \mathbf{V}$, $\mathbf{u}$ is zero on the non-empty set of Dirichlet boundary nodes $\mathcal{N}(\Gamma)$, where $\Gamma \subset \partial\Omega$. We can easily handle non-zero boundary data $\mathbf{u}(x) = \mathbf{g}(x)$ for $x \in \mathcal{N}(\Gamma)$ by extending $\mathbf{g}$ to all nodes and write $\mathbf{u} = \mathbf{u}_0 + \mathbf{g}$, where $\mathbf{u}_0 \in \mathbf{V}$ solves Eq. (5) with modified right hand side $(\tilde{\mathbf{f}}, \mathbf{v}) := (\mathbf{f}, \mathbf{v}) - (\mathbf{K}\mathbf{g}, \mathbf{v})$.

Next we make some assumptions on the operator $\mathbf{K}$.

**Assumption 2.1.** The operator $\mathbf{K}$

1. is bounded and coercive on $\mathbf{V}$ with respect to the $\mathbf{L}$-norm, i.e. there are constants $0 < \alpha \le \beta < \infty$ such that

$$\alpha |\mathbf{v}|_{\mathbf{L}}^2 \le (\mathbf{K}\mathbf{v}, \mathbf{v}) \le \beta |\mathbf{v}|_{\mathbf{L}}^2 \tag{6}$$

   for all $\mathbf{v} \in \mathbf{V}$, and
2. can be written as a sum $\mathbf{K} = \sum_{x \in \mathcal{N}} \mathbf{K}_x$ of operators $\mathbf{K}_x : \hat{\mathbf{V}} \to \hat{\mathbf{V}}$, where $\mathbf{K}_x$ are symmetric positive semi-definite and have support on $x$ and nodes adjacent to $x$.

The operator $\mathbf{K}$ is symmetric as a consequence of $\mathbf{K}_x$ being symmetric and the bilinear form $(\mathbf{K}\cdot, \cdot)$ is an inner product on $\mathbf{V}$ because of the norm equivalence in Eq. (6). Therefore, Eq. (5) has a unique solution. With $\mathbf{K}_\omega = \sum_{x \in \mathcal{N}(\omega)} \mathbf{K}_x$ we define the following (semi-)norms $|\mathbf{v}|_{\mathbf{K}} = (\mathbf{K}\mathbf{v}, \mathbf{v})^{1/2}$ and $|\mathbf{v}|_{\mathbf{K},\omega} = (\mathbf{K}_\omega \mathbf{v}, \mathbf{v})^{1/2}$. We now give three examples of system matrices $\mathbf{K}$ that we consider in this work.

**Example 2.2** (*Heat Conductivity*)**.** Since this is a scalar example we drop the bold face notation. The same goes for the corresponding (first) numerical example of this model in Section 5. Let $n = 1$ and $u$ be the sought temperature distribution in the nodes of the network. We define $K_x$ by

$$(K_x v, w) = \frac{1}{2} \sum_{y \sim x} \gamma_{xy} \frac{(v(x) - v(y))(w(x) - w(y))}{|x - y|},$$

where $0 < \gamma_{xy} < \infty$ is heat conductivity on the edges. Assumption 2.1 is satisfied with $\alpha = \min_{x \sim y} \gamma_{xy}$ and $\beta = \max_{x \sim y} \gamma_{xy}$. The right hand side $f$ represents an external heat source.

**Example 2.3** (*Spring Model*)**.** Let $d = n = 3$, and $\partial_{xy} = |x - y|^{-1}(x - y)$ be the unit direction vector for edge $\{x, y\}$, then we can define

$$(\mathbf{K}_x \mathbf{v}, \mathbf{w}) = \frac{1}{2} \sum_{y \sim x} \gamma_{xy} \frac{((\mathbf{v}(x) - \mathbf{v}(y))^T \partial_{xy})((\mathbf{w}(x) - \mathbf{w}(y))^T \partial_{xy})}{|x - y|}, \tag{7}$$

where $0 < \gamma_{xy} < \infty$ measures the elasticity of the edges. The upper bound of the first assumption in Assumption 2.1 is satisfied with $\beta = \max_{x \sim y} \gamma_{xy}$ since $\partial_{xy}$ has unit length. Whether the lower bound is satisfied or not depends on the geometry of the network. At least $d$ nodes need to be in $\Gamma$ and they have to span a plane. Additionally, the network needs to be a rigid structure. The value of $\alpha$ depends on $\gamma_{xy}$ and on the structural rigidity of the network. We seek the displacement $\mathbf{u}$ of the nodes under the load $\mathbf{f}$.

**Example 2.4** (*Fiber Network Model*)**.** Example 2.3 can be expanded to represent beams by adding bending stiffness to the edges. A linearized Euler–Bernoulli model can be written on a similar form as (7). For $k = 1, 2$, then

$$\begin{aligned} (\mathbf{K}_x^{(k)} \mathbf{v}, \mathbf{w}) &= \sum_{\substack{x \sim y \wedge x \sim z \\ y \neq z}} \gamma_{xyz}^{(k)} \frac{|x - y| + |x - z|}{2} g_{xyz}(\mathbf{v}) g_{xyz}(\mathbf{w}), \\ g_{xyz}(\mathbf{v}) &= \frac{(\mathbf{v}(y) - \mathbf{v}(x)) \cdot \eta_{xyz}^{y,(k)}}{|x - y|} + \frac{(\mathbf{v}(z) - \mathbf{v}(x)) \cdot \eta_{xyz}^{z,(k)}}{|x - z|}, \end{aligned} \tag{8}$$

where $\eta_{xyz}^{y,(1)} = \eta_{xyz}^{z,(1)}$ is a unit vector orthogonal to both $\partial_{xy}$ and $\partial_{xz}$, and $\eta_{xyz}^{r,(2)} = \partial_{xr} \times \eta_{xyz}^{r,(1)}$ for $r = y, z$. Adding components $\mathbf{K}_x^{(1)}$ and $\mathbf{K}_x^{(2)}$ to (7) results in an operator that capture tensile strains and bending resistance. For more details about this network model, see [2].

## 3. Coarse scale representation

The aim of this work is to derive an upscaled representation of the spatial network model problem (5) using the LOD methodology. This representation should have significantly fewer degrees of freedom, but still yield an accurate solution to the original problem. In this section, using a construction first presented in [16], we define a coarse scale finite element representation that will be used to form the LOD space. The construction involves three main steps. First, we make assumptions on the spatial network, since not all networks allow for accurate upscaling. In essence, the network should resemble a homogeneous material on the coarse scale. Second, a finite element mesh and coarse function space is introduced on the coarse scale. Third, we introduce a novel idempotent interpolation operator onto the finite element function space and establish the corresponding interpolation error bound.

### 3.1. Network assumptions

Four assumptions on the network are made, guaranteeing homogeneity, connectivity, and locality on a coarse scale. As a technical tool for the assumptions, and later for the definition of the finite element mesh, we define boxes $B_R(x) \subset \Omega$ with side length $2R$ and midpoint $x = (x_1, \dots, x_d)$ as follows. Let

$$B_R(x) = [x_1 - R, x_1 + R) \times \cdots \times [x_d - R, x_d + R),$$

but if $x_i + R = l_i$, we replace $[x_i - R, x_i + R)$ with $[x_i - R, x_i + R]$.

From [16] we recall the following network assumptions.

**Assumption 3.1** (*Network Assumptions*)**.** There is a length-scale $R_0$ and a uniformity constant $\sigma$, so that

1. (homogeneity) for all $R \geq R_0$, it holds that
$$\max_{B_R(x) \subset \Omega} |1|^2_{M,B_R(x)} \leq \sigma \min_{B_R(x) \subset \Omega} |1|^2_{M,B_R(x)},$$
2. (locality) the edge length $|x - y| < R_0$ for all edges $\{x, y\} \in \mathcal{E}$,
3. (boundary density) for any $y \in \Gamma$, there is an $x \in \mathcal{N}(\Gamma)$ such that $|x - y| < R_0$.
4. (connectivity) for all $R \geq R_0$ and $x \in \Omega$, there is a connected subgraph $\bar{\mathcal{G}} = (\bar{\mathcal{N}}, \bar{\mathcal{E}})$ of $\mathcal{G}$, that contains
   (a) all edges with one or both endpoints in $B_R(x)$,
   (b) only edges with endpoints contained in $B_{R+R_0}(x)$.

The four assumptions can be interpreted at scale $R_0$ as follows. The homogeneity assumption implies that the spatial network has homogeneous density over the domain in terms of the $M$-norm mass. The locality assumption says that edges connect only nodes close to each other, while the boundary density requires that the boundary conditions are given close enough to nodes. The connectivity assumption guarantees that nodes close to each other spatially are also close to each other in the network.

Under the assumptions above, the following Friedrichs and Poincaré inequalities are proven in [16].

**Lemma 3.2** (*Friedrichs and Poincaré Inequalities*)**.** *If Assumption 3.1 holds, then there is a $\mu < \infty$ such that for all $R \geq R_0$ and $x \in \Omega$ for which*

- *(Friedrichs) $B_R(x)$ contains boundary nodes, it holds that*
$$|v|_{M,B_R(x)} \leq \mu R |v|_{L,B_{R+R_0}(x)},$$
*for all $v \in V$,*
- *(Poincaré) $B_R(x)$ may or may not contain boundary nodes, it holds that*
$$|v - c|_{M,B_R(x)} \leq \mu R |v|_{L,B_{R+R_0}(x)},$$
*for some constant function $c = c(R, x, v)$, for all $v \in \hat{V}$.*

The constant $\mu$ enters the interpolation bounds and consequently affects the accuracy of the homogenization method presented in Section 4. For simple networks, such as regular grids, the constant can be shown to be small, while for most networks, theoretical bounds are generally difficult to obtain. The constant $\mu$ can, however, be estimated numerically.

As an illustration on how to estimate $\mu$ in the Poincaré case, we pick an $R \geq R_0$ and an $x \in \Omega$. We start from the eigenvalue problem $\lambda_2 = \min_{v \in \hat{V} : (\bar{M}v, 1) = 0} \frac{|v|^2_{\bar{L}}}{|v|^2_{\bar{M}}}$, where $\bar{M}$ and $\bar{L}$ are the corresponding norms for the graph $\bar{\mathcal{G}}$ in Assumption 3.1. Note that $\lambda_2$ is the second smallest eigenvalue associated with the Rayleigh quotient $\frac{|\cdot|^2_{\bar{L}}}{|\cdot|^2_{\bar{M}}}$, since the constant $c$ is an eigenvector for the only zero eigenvalue. The connectivity of $\bar{\mathcal{G}}$ implies that $\lambda_2$ is non-zero. We get

$$|v - c|^2_{M,B_R(x)} \leq (\bar{M}(v - c), v - c) \leq \lambda_2^{-1} |v|^2_{L,B_{R+R_0}(x)}. \tag{9}$$

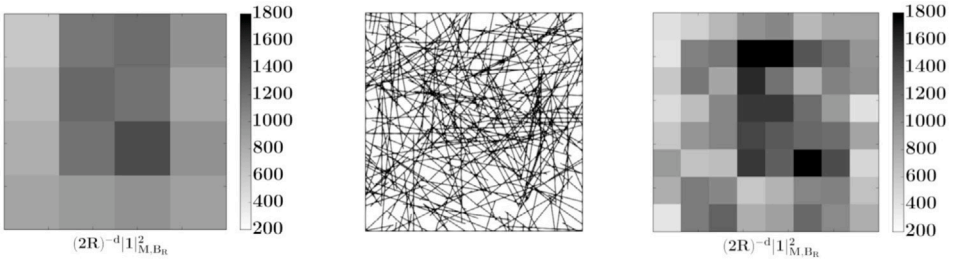


**Fig. 3.** Illustration of the homogeneity equation in Assumption 3.1 for a random network generated on the square $[0, 0.1]^2$ with edge length $r = 0.05$ and density $\rho_{\text{gen}} = 10^3$ (center) for a grid of $B_R$ with $R = 1.25 \cdot 10^{-2}$ (left) and $R = 6.25 \cdot 10^{-3}$ (right).

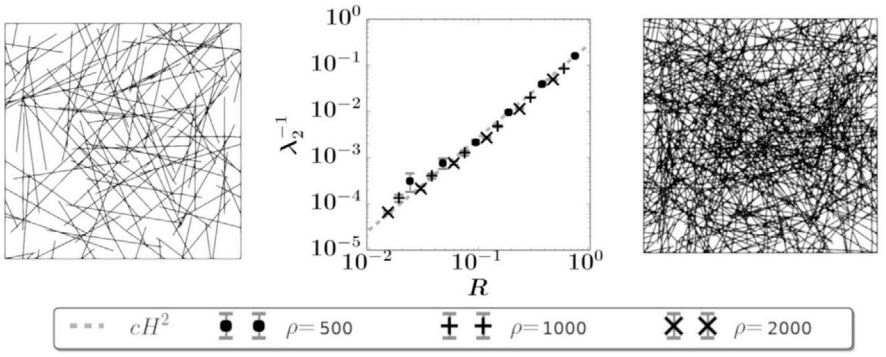


**Fig. 4.** The eigenvalue $\lambda_2^{-1}$ for different networks with varying sizes and densities. Each combination is analyzed ten times, with the mean (marker) and standard deviation (feet) results presented. Comparable networks to the one in Fig. 3 are shown with $\rho_{\text{gen}} = 5 \cdot 10^2$ (left) and $2 \cdot 10^3$ (right).

Thus, $\mu^2 R^2$ is bounded by the maximum $\lambda_2^{-1}$ attained for any $R \geq R_0$ and $x \in \Omega$. A similar eigenvalue problem can be formulated for the Friedrichs case. Next, we illustrate by a number of examples how the connectivity and homogeneity constants can be estimated numerically based on this eigenvalue problem.

**Example 3.3** (*Numerical Estimates of Homogeneity and Connectivity*)**.** To visualize the homogeneity and connectivity assumptions of Assumption 3.1, several random square networks are generated and evaluated. The analyzed networks are generated by randomly placing edges with a fixed length in a domain. Three attributes categorize each network: the side length $R$ of the domain, the length $r$ of the edges placed, and a density $\rho_{\text{gen}}$. The networks are generated in three steps. First, the edges are randomly placed with their midpoints in the extended domain $[-r, R + r]^2$ with a random rotation. This extension guarantees uniform coverage, and any part of an edge placed outside the network domain $[0, R]^2$ is removed. Edges are placed until the total edge length of the network is $\rho_{\text{gen}} R^2$. The second step is adding a node in every point where two edges intersect. The final step removes any loose edges and combines nodes closer than $0.01r$ to guarantee a lower bound on the edge lengths. The largest remaining connected network is kept. An illustration of the homogeneity assumption is shown in Fig. 3 for a network with parameter $R = 0.1, r = 0.05$, and $\rho_{\text{gen}} = 10^3$. This figure shows how the mean value of the local density $\frac{|1|^2_{M,B_R}}{(2R)^2}$ stays similar ($\approx \rho_{\text{gen}}$) when $R$ is halved but varies more throughout the network. The connectivity property is analyzed for multiple networks with multiple parameters, and a composite of the results is presented in Fig. 4. We see that $\lambda_2^{-1}$ scales with $R^2$ and thus the connectivity assumption holds for the networks in the interval of $R$ analyzed with $\mu^2 \approx 10$.

### 3.2. Coarse mesh

With the network embedded in a domain $\Omega$ we can introduce a family of meshes over $\Omega$ for the coarse discretization. The elements have to be larger than the length-scale $R_0$ of the network introduced in the previous section. To help convey the main message of the paper, we choose a simple mesh of hypercubes (squares for $d = 2$, and cubes for $d = 3$, etc.). For a general polygonal or polyhedral domain, triangles or tetrahedrons can be used. The main difference in the analysis is that constants also will depend on the shape regularity parameter of the mesh.

Let $\mathcal{T}_H$ be subdivisions of $\Omega$ into elements of side length $H$ as follows,

$$\mathcal{T}_H = \{B_{H/2}(x) \ : \ x = (x_1, \dots, x_d) \in \Omega \text{ and } H^{-1}x_i + 1/2 \in \mathbb{Z} \text{ for } i = 1, \dots, d\}.$$

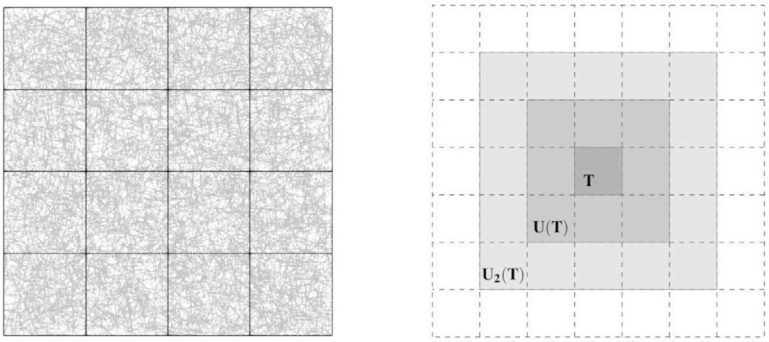


**Fig. 5.** A partition $\mathcal{T}_H$, with $H = 1/4$ on the unit square (left) and an illustration showing the recursive operator $U_k$ (right).

We require that $l_1, \dots, l_d$ are integer multiples of $H$ so that the mesh covers $\Omega$. The box definition $B_R(x)$ from the previous section is used here. This makes $\mathcal{T}_H$ a true partition so that each point in $\Omega$ is included in exactly one element. An illustration of such a partition is presented in Fig. 5 (left). We assume that the boundary segments $\Gamma$ are union of mesh element edges (or faces) so that a conforming finite element function space can be defined. Since we define elements $B_{H/2}$, with half side length in the subscript, but the length-scales $B_R$ using the full side length, it is natural to define a mesh length-scale,

$$H_0 = 2R_0.$$

The elements must be larger than the mesh length-scale $H_0$ of the network. In fact, to define a stable idempotent quasi-interpolation operator, we require that

$$H \geq 4d H_0. \tag{10}$$

For a motivation of this lower bound, see the proof of Lemma 3.4. Thus, these meshes are coarse compared to the homogeneity and connectivity length-scale $H_0$. Note, we do not require that the mesh nodes coincide with the network nodes.

To handle patches of elements in a mesh $\mathcal{T}_H$, we introduce the notation $U$. We let, for $\omega \subset \Omega$,

$$U(\omega) = \{x \in \Omega \ : \ \exists T \in \mathcal{T}_H \ : \ x \in T, T \cap \overline{\omega} \neq \emptyset\}.$$

For instance, $U(T)$ contains the points both in $T$ and in the elements adjacent to $T$. Recursively, we define $U_j(\omega) = U_{j-1}(U(\omega))$ with $U_1 = U$. An illustration of $T$, $U(T)$, and $U_2(T)$ can be found in Fig. 5 (right).

### 3.3. Interpolation

In this section, we define the function space to be used for the coarse representation and an interpolation operator from the functions on the network to this coarse space. The interpolation operator is of Scott–Zhang type (see [17]) and is defined by use of an $M$-dual basis. By showing that the dual basis functions are appropriately bounded, we obtain the accuracy and stability result for the interpolation operator in Lemma 3.5. A Scott–Zhang type operator is used here since it is important for the analysis of the LOD method that the interpolation operator is idempotent.

Let $\hat{\mathcal{Q}}_H$ denote the continuous real functions over $\Omega$ whose restriction to $T \in \mathcal{T}_H$ can be written as a linear combination of $z = (z_1, \dots, z_d) \mapsto z^\alpha$ for multi-index $\alpha$ with $\alpha_i \in \{0, 1\}$, $i = 1, \dots, d$. For $d = 2$, this is the space of functions that are bilinear on each element. The functions satisfying the boundary conditions are $\mathcal{Q}_H = \{p \in \hat{\mathcal{Q}}_H \ : \ p|_\Gamma = 0\}$. We let $\hat{V}_H$ and $V_H$ be the restriction of $\hat{\mathcal{Q}}_H$ and $\mathcal{Q}_H$ to the nodes in the network.

From this point on, we study a fixed $H$. Denote by $\varphi_1, \dots, \varphi_m \in \hat{V}_H$ the Lagrange finite element basis functions and $y_1, \dots, y_m$ the corresponding mesh nodes. An illustration of a $\varphi_i$ function can be found in Fig. 6. We assume that the basis functions are sorted so that the basis functions $\varphi_1, \dots, \varphi_{m_0}$, $m_0 < m$ span $V_H$ that vanish on $\Gamma$. For each mesh node $y_k$, we denote by $T_k$ the unique element that contains it and define $\psi_k \in \hat{V}_H(T_k)$ that satisfies

$$(M_{T_k}\psi_k, \varphi_\ell) = \delta_{k\ell} \tag{11}$$

for all $\ell = 1, \dots, m$. Note that the scalar product is still the Euclidean scalar product on the network, i.e. only the values of the functions $\varphi_\ell$ and $\psi_k$ in the network nodes affect the product.

The interpolation operator is then defined by

$$\mathcal{I}v = \sum_{k=1}^{m_0} (M_{T_k}\psi_k, v)\varphi_k.$$

We let the subscript $z$ of a constant $C_z$ indicate a dependency on a constant $z$, where the exact value of $C_z$ may differ (by some generic constant).

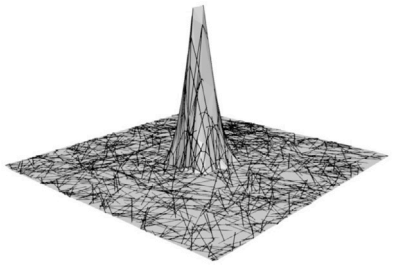

**Fig. 6.** A two-dimensional network (black) displaced to the discrete function values of the $\varphi$ basis function. The gray shading is a triangulation of the displaced network for illustrative purposes.

**Lemma 3.4** (*Dual Basis Norm Bound*). *If Assumption 3.1 holds and* $H \geq 4d\,H_0$, *then for any* $S \in \mathcal{T}_H$

$$\left(|\varphi_k|_{M,S} + H|\varphi_k|_{L,S}\right)|\psi_k|_{M,T_k} \leq C_d\sigma^{1/2} \tag{12}$$

*for mesh nodes* $k = 1, \dots, m$. *The proof of this identity is provided in the Appendix.*

With the above result on the dual basis norm bound, we can show the following interpolation bound.

**Lemma 3.5.** *If Assumption 3.1 holds and* $H \geq 4d\,H_0$, *then for* $v \in V$ *and all* $T \in \mathcal{T}_H$,

$$H^{-1}|v - \mathcal{I}v|_{M,T} + |\mathcal{I}v|_{L,T} \leq C_{d,\mu,\sigma}|v|_{L,U_3(T)}. \tag{13}$$

This is an element local version of [16, Lemma 5.2] with a different choice of nodal variable $v \mapsto (M_{T_k}\psi_k, v)$ for the interpolation operator. In [16], a Clément interpolation operator is used, while a Scott–Zhang interpolation operator is used here. The proof can be used almost verbatim to prove this element local version, with the exceptions to leave out the summation over all elements in the end and apply Lemma 3.4 in the third inequality of equation 5.5 in [16].

## 4. Numerical homogenization

Given the spatial network model and a coarse scale finite element space, the aim is to derive an accurate upscaled representation of the model problem. This is accomplished by using the localized orthogonal decomposition (LOD) technique originally developed for numerical homogenization of elliptic partial differential equations with heterogeneous data, see [8,9]. An accurate representation is achieved by decoupling the fine scale computations into local subproblems and thereby constructing a multiscale basis that captures the data variation. The heterogeneities present in the spatial network setting come from the geometry of the graph and the spatially varying weights. With the results from Section 3, we can derive the LOD method for the model problem defined in Eq. (5). We let $\boldsymbol{\mathcal{I}} : \mathbf{V} \to \mathbf{V}$ be defined as $\boldsymbol{\mathcal{I}}\mathbf{v} = [\mathcal{I}v_1, \dots, \mathcal{I}v_n]$ and introduce a fine scale space

$$\mathbf{W} = \ker(\boldsymbol{\mathcal{I}}) = \{\mathbf{v} \in \mathbf{V} \,:\, \boldsymbol{\mathcal{I}}\mathbf{v} = 0\}.$$

### 4.1. Ideal multiscale method

The multiscale space $\mathbf{V}_H^{\text{ms}}$ is defined as the orthogonal complement of $\mathbf{W}$ with respect to the inner product induced by $\mathbf{K}$. For every $\mathbf{v} \in \mathbf{V}$ we define a fine scale projection operator $\mathbf{Q} : \mathbf{V} \to \mathbf{W}$ such that

$$(\mathbf{KQv}, \mathbf{w}) = (\mathbf{Kv}, \mathbf{w}) \tag{14}$$

for all $\mathbf{w} \in \mathbf{W}$.

**Definition 4.1.** The ideal multiscale space is defined as

$$\mathbf{V}_H^{\text{ms}} = \{(1 - \mathbf{Q})\mathbf{v} \,:\, \mathbf{v} \in \mathbf{V}\}.$$

Any vector $\mathbf{v} \in \mathbf{V}$ can be decomposed into

$$\mathbf{v} = (\mathbf{v} - \mathbf{Qv}) + \mathbf{Qv} \in \mathbf{V}_H^{\text{ms}} \oplus \mathbf{W}$$

with the two terms being $\mathbf{K}$-orthogonal. The ideal multiscale approximation $\mathbf{u}_H$ of $\mathbf{u}$ fulfills: find $\mathbf{u}_H \in \mathbf{V}_H^{\text{ms}}$ such that for all $\mathbf{v} \in \mathbf{V}_H^{\text{ms}}$

$$(\mathbf{Ku}_H, \mathbf{v}) = (\mathbf{f}, \mathbf{v}). \tag{15}$$

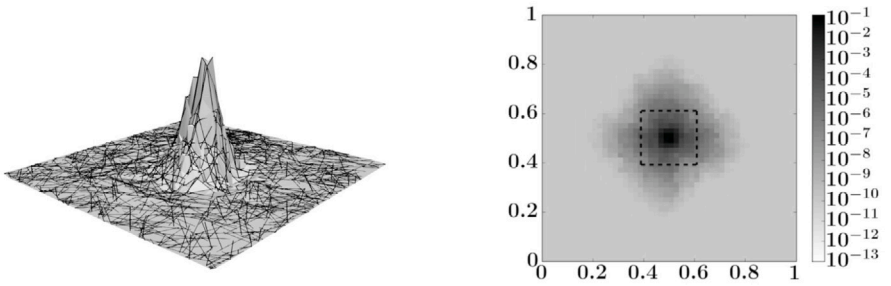


**Fig. 7.** The bilinear function, $\varphi$, in Fig. 6 with an ideal fine scale correction, i.e. $(1-\mathbf{Q})\boldsymbol{\varphi}$ for a heat conductivity problem. The left figure is comparable to Fig. 6, and the right shows $(1-\mathbf{Q})\boldsymbol{\varphi}$ in the entire domain with the area of the left marked with the dashed lines.

**Lemma 4.2.** *The error in the approximate solution $\mathbf{u}_H$, defined in Eq. (15), fulfills*

$$|\mathbf{u}-\mathbf{u}_H|_{\mathbf{K}} \leq C_{\alpha,d,\mu,\sigma} H |\mathbf{f}|_{\mathbf{M}^{-1}},$$

*where* $|\mathbf{f}|^2_{\mathbf{M}^{-1}} = (\mathbf{M}^{-1}\mathbf{f},\mathbf{f})$.

**Proof.** The error $\mathbf{u}-\mathbf{u}_H \in \mathbf{W}$ is bounded by

$$\begin{aligned}
|\mathbf{u}-\mathbf{u}_H|^2_{\mathbf{K}} &= (\mathbf{K}\mathbf{u},\mathbf{u}-\mathbf{u}_H)\\
&= (\mathbf{f},\mathbf{u}-\mathbf{u}_H)\\
&\leq |\mathbf{f}|_{\mathbf{M}^{-1}} |\mathbf{u}-\mathbf{u}_H - \mathcal{I}(\mathbf{u}-\mathbf{u}_H)|_{\mathbf{M}}\\
&\leq C_{\alpha,d,\mu,\sigma} H |\mathbf{f}|_{\mathbf{M}^{-1}} |\mathbf{u}-\mathbf{u}_H|_{\mathbf{K}},
\end{aligned}$$

where Lemma 3.5 is used in all coordinate directions and the overlap of subregions $U_3(T)$ are hidden in $C_{\alpha,d,\mu,\sigma}$. The lemma follows after division by $|\mathbf{u}-\mathbf{u}_H|_{\mathbf{K}}$. □

For the method to be computationally feasible we need to localize the fine scale correction operators. To do this, we first decompose the computation of $\mathbf{Q}$ to the elements $T \in \mathcal{T}_H$. We define $\mathbf{Q}_T : \mathbf{V} \to \mathbf{W}$, such that for any $\mathbf{v} \in \mathbf{V}$

$$(\mathbf{K}\mathbf{Q}_T\mathbf{v},\mathbf{w}) = (\mathbf{K}_T\mathbf{v},\mathbf{w}) \tag{16}$$

for all $\mathbf{w} \in \mathbf{W}$. By this choice, $\mathbf{Q}_T\mathbf{v}$ is independent of the values of $\mathbf{v}$ in points not adjacent to nodes in $T$. Note that $\mathbf{Q} = \sum_{T\in\mathcal{T}_H} \mathbf{Q}_T$ since $\mathbf{K}_T = \sum_{x\in T} \mathbf{K}_x$ sums up to $\mathbf{K}$.

### 4.2. The LOD method

With the fine scale correction decomposed into element components, we want to localize the computation of those components to element patches. Let

$$\mathbf{W}(\omega) = \{\mathbf{w} \in \mathbf{W} \ : \ \mathbf{w}(x) = 0 \text{ for } x \in \mathcal{N}(\Omega \setminus \omega)\}$$

and let $\mathbf{Q}^k_T\mathbf{v} \in \mathbf{W}(U_k(T))$ be the solution to

$$(\mathbf{K}\mathbf{Q}^k_T\mathbf{v},\mathbf{w}) = (\mathbf{K}_T\mathbf{v},\mathbf{w}) \tag{17}$$

for all $\mathbf{w} \in \mathbf{W}(U_k(T))$. We sum the contributions over the elements to get the full truncated fine scale projection operator $\mathbf{Q}^k\mathbf{v} = \sum_{T\in\mathcal{T}_H} \mathbf{Q}^k_T\mathbf{v}$. By this construction, $\mathbf{Q}^k$ is an approximation of $\mathbf{Q}$ computed on element patches.

To define the truncated LOD space, we define coarse basis functions for the free nodes. Let $\boldsymbol{\varphi}_j$ for $j = 1,2,\dots,nm_0$ enumerate the basis functions that span the range of $\mathcal{I}$. We define them as $\boldsymbol{\varphi}_1 = [\varphi_1,0,\dots,0]$, $\boldsymbol{\varphi}_2 = [\varphi_2,0,\dots,0],\dots,\boldsymbol{\varphi}_{m_0} = [\varphi_{m_0},0,\dots,0]$, $\boldsymbol{\varphi}_{m_0+1} = [0,\varphi_1,0,\dots,0]$, to $\boldsymbol{\varphi}_{nm_0} = [0,\dots,0,\varphi_{m_0}]$.

**Definition 4.3.** The truncated LOD space is given by

$$\mathbf{V}^{\mathrm{ms},k}_H = \operatorname{span}\left(\left\{\boldsymbol{\varphi}_j - \sum_{T\in\mathcal{T}_H} \mathbf{Q}^k_T\boldsymbol{\varphi}_j \ : \ j = 1,\dots,nm_0\right\}\right)$$

and the LOD approximation by: find $\mathbf{u}^k_H \in \mathbf{V}^{\mathrm{ms},k}_H$ such that for all $\mathbf{v} \in \mathbf{V}^{\mathrm{ms},k}_H$ (see Fig. 7),

$$(\mathbf{K}\mathbf{u}^k_H,\mathbf{v}) = (\mathbf{f},\mathbf{v}). \tag{18}$$

**Remark 4.4** (*Nonlinear Problems*). Nonlinear problems, where $\mathbf{K}$ depends on $\mathbf{u}$, can be treated efficiently if the nonlinearity is localized to the support of a small number of correctors, since only these correctors need to be recomputed between the nonlinear iterations. A more general and systematic approach is to compute error indicators for the correctors as in [18] and recompute only the correctors with sufficiently large error in every iteration.

### 4.3. Decay of fine scale correctors

In order for $\mathbf{u}_H^k$ to be a good approximation of $\mathbf{u}$ for small values of $k$ we need to show that $\mathbf{Q}_T\boldsymbol{\varphi}_j$ decays quickly away from $T$. This is done by following ideas presented in [16,19], using Lemma 3.5 and a discrete analog to the product rule.

The idea is to approximate the fine scale projection $\mathbf{Q}$ using an iterative domain decomposition technique that spreads information locally in each iteration. By proving that the method converges quickly we can also draw conclusions about the decay of the $\mathbf{Q}_T\boldsymbol{\varphi}_j$.

For points $x \in \Omega$, let $U(x)$ be used as short-hand notation for $U(\{x\})$. In particular, if $y_k$ is a mesh node then $U(y_k)$ is the node patch. We let $\mathbf{V}_j = \mathbf{V}(U(y_j))$ be the space of functions that vanish outside the node patch for mesh nodes $j = 1, \dots, m$ (including the fixed mesh nodes $m_0 + 1, m_0 + 2 \dots, m$). The fine scale space $\mathbf{W}$ is decomposed into overlapping subspaces

$$\mathbf{W}_j = (1 - \boldsymbol{\mathcal{I}})\mathbf{V}_j = \{\mathbf{v} - \boldsymbol{\mathcal{I}}\mathbf{v} \ : \ \mathbf{v} \in \mathbf{V}_j\}.$$

The relation $\mathbf{W}_j \subset \mathbf{W}$ holds since $\boldsymbol{\mathcal{I}}$ is idempotent. Since the scalar basis $\{\varphi_j\}_{j=1,\dots,m}$ is a partition of unity on $\mathcal{N}$, any $\mathbf{w} \in \mathbf{W}$ can be written as

$$\mathbf{w} = \sum_{j=1}^{m} (1 - \boldsymbol{\mathcal{I}})(\varphi_j \mathbf{w}) \quad \text{with} \quad (1 - \boldsymbol{\mathcal{I}})(\varphi_j \mathbf{w}) \in \mathbf{W}_j,$$

where $\varphi_j \mathbf{w} = [\varphi_j w_1, \dots, \varphi_j w_n]$. Remember that $(\boldsymbol{\mathcal{I}}\mathbf{v})(y_j)$ is computed by taking a weighted average of $\mathbf{v}$ in element $T_j$ with $y_j \in T_j$. Therefore, $\boldsymbol{\mathcal{I}}\mathbf{v}$ has a slightly larger support than $\mathbf{v}$. More precisely, any $\mathbf{w}_j \in \mathbf{W}_j$ fulfills

$$\mathbf{w}_j \in \mathbf{V}(U_1(\hat{T}_j)) \cap \mathbf{W}, \tag{19}$$

where $\hat{T}_j$ is an element adjacent to the node $y_j$.

Now let $\mathbf{P}_j \ : \ \mathbf{V} \to \mathbf{W}_j$ define the projection such that for any $\mathbf{v} \in \mathbf{V}$ and all $\mathbf{w} \in \mathbf{W}_j$

$$(\mathbf{K}\mathbf{P}_j\mathbf{v}, \mathbf{w}) = (\mathbf{K}\mathbf{v}, \mathbf{w}).$$

The operator $\mathbf{P} = \sum_{j=1}^{m} \mathbf{P}_j$ is a preconditioner for $\mathbf{Q}$, and it is important that it only spreads information a few layers of coarse elements in each application by Eq. (19).

Next, we investigate some further properties of $\mathbf{P}$. The following discrete analogue of a product rule (see [16] for a proof),

$$|v\varphi_k|_{L,T}^2 \leq 2\left(H^{-2}|v|_{M,T}^2 + |v|_{L,T}^2\right), \quad k = 1, \dots, m, \quad T \in \mathcal{T}_H, \tag{20}$$

is used to the prove the following identities.

**Lemma 4.5.** *Every decomposition* $\mathbf{w} = \sum_{j=1}^{m} \mathbf{w}_j$ *with* $\mathbf{w}_j \in \mathbf{W}_j$ *satisfies*

$$|\mathbf{w}|_{\mathbf{K}}^2 \leq C_2 \sum_{j=1}^{m} |\mathbf{w}_j|_{\mathbf{K}}^2$$

*and the particular decomposition* $\mathbf{w}_j = (1 - \boldsymbol{\mathcal{I}})(\varphi_j \mathbf{w})$ *satisfies*

$$\sum_{j=1}^{m} |\mathbf{w}_j|_{\mathbf{K}}^2 \leq C_1 |\mathbf{w}|_{\mathbf{K}}^2.$$

*The proof of this Lemma can be found in the* Appendix.

Using Lemma 4.5 one can show the following norm equivalence, where we refer to Lemma 3.1 in [5] for a proof of the first statement and the appendix of [16] for a proof of the second statement.

**Lemma 4.6.** *The following norm equivalence holds*

$$C_1^{-1}|\mathbf{w}|_{\mathbf{K}}^2 \leq (\mathbf{K}\mathbf{P}\mathbf{w}, \mathbf{w}) \leq C_2 |\mathbf{w}|_{\mathbf{K}}^2$$

*for all* $\mathbf{w} \in \mathbf{W}$. *Furthermore, with* $\nu = (C_2 + C_1^{-1})^{-1}$ *and* $\mathbf{w} \in \mathbf{W}$, *it holds*

$$\sup_{\mathbf{w} \in \mathbf{W}} \frac{|(1 - \nu\mathbf{P})\mathbf{w}|_{\mathbf{K}}}{|\mathbf{w}|_{\mathbf{K}}} \leq \gamma < 1,$$

*where* $\gamma \leq \frac{C_2}{C_2 + C_1^{-1}}$.

We now define an approximation $\mathbf{R}_T^k : \mathbf{V} \to \mathbf{W}$ to $\mathbf{Q}_T$ by the iteration,

$$\mathbf{R}_T^k \mathbf{v} = \mathbf{R}_T^{k-1}\mathbf{v} + \nu \mathbf{P}(\mathbf{Q}_T - \mathbf{R}_T^{k-1})\mathbf{v}, \quad k \geq 1, \tag{21}$$

with $\mathbf{R}_T^0 = 0$ and a relaxation parameter $\nu > 0$. First we note that $\mathbf{R}_T^k \mathbf{v}$ is computable without explicitly forming $\mathbf{Q}_T \mathbf{v}$ since $\mathbf{P}_j \mathbf{Q}_T \mathbf{v} \in \mathbf{W}_j$ solves

$$(\mathbf{K}\mathbf{P}_j \mathbf{Q}_T \mathbf{v}, \mathbf{w}_j) = (\mathbf{K}\mathbf{Q}_T \mathbf{v}, \mathbf{w}_j) = (\mathbf{K}_T \mathbf{v}, \mathbf{w}_j)$$

for all $\mathbf{w}_j \in \mathbf{W}_j$. We further conclude that $\mathbf{R}_T^k$ is local. The right hand side $\mathbf{K}_T \mathbf{v}$ has support on $U_1(T)$. Since functions in $\mathbf{W}_j$ have support on $U_1(\hat{T}_j)$ according to Eq. (19) only a few of the corresponding projections $\mathbf{P}_j$ will be non-zero. More precisely $\mathbf{R}_T^1$ will have support on $U_3(T)$ and in general

$$\operatorname{supp}(\mathbf{R}_T^k) \subset U_{3k}(T).$$

We will use this property when we show that $\mathbf{Q}_T$ decays exponentially. The approximation $\mathbf{R}_T^k$ of $\mathbf{Q}_T$ fulfills the error bound

$$(\mathbf{Q}_T - \mathbf{R}_T^k)\mathbf{v} = (1 - \nu\mathbf{P})(\mathbf{Q}_T - \mathbf{R}_T^{k-1})\mathbf{v} = (1 - \nu\mathbf{P})^k \mathbf{Q}_T \mathbf{v}. \tag{22}$$

Altogether we get the following approximation result.

**Lemma 4.7.** *It holds*

$$|(\mathbf{Q}_T - \mathbf{R}_T^k)\mathbf{w}|_{\mathbf{K}} \leq \exp(-k(2C_1C_2)^{-1})|\mathbf{w}|_{\mathbf{K},T}.$$

**Proof.** Using Eq. (22) and Lemma 4.6 we conclude

$$|(\mathbf{Q}_T - \mathbf{R}_T^k)\mathbf{w}|_{\mathbf{K}} \leq \gamma^k |\mathbf{Q}_T \mathbf{w}|_{\mathbf{K}} \leq \gamma^k |\mathbf{w}|_{\mathbf{K},T}.$$

Since $\gamma \leq \frac{C_2}{C_2 + C_1^{-1}}$ we have that $\log(\gamma^{-1}) \geq (2C_1C_2)^{-1}$ by Maclaurin expansion and therefore

$$\gamma^k = \exp(-k\log(\gamma^{-1})) \leq \exp(-k(2C_1C_2)^{-1}). \quad \square$$

In the last technical lemma we show that the error $\mathbf{Q}\mathbf{v} - \mathbf{Q}^k\mathbf{v}$ decays exponentially in $k$.

**Lemma 4.8.** *For any $\mathbf{v} \in \mathbf{V}$ it holds*

$$|(\mathbf{Q} - \mathbf{Q}^k)\mathbf{v}|_{\mathbf{K}} \leq C_{\alpha,\beta,d,\mu,\sigma} k^{d/2} \exp(-k(6C_1C_2)^{-1})|\mathbf{v}|_{\mathbf{K}}.$$

*The proof is provided in the* Appendix.

With Lemma 4.8, the use of $\mathbf{Q}^k$ instead of $\mathbf{Q}$ is thoroughly motivated. Moreover, with exponential decay the element patches can be small and still be representative. Now all that is left is to provide the final a priori estimate for the localized LOD approximation $\mathbf{u}_H^k$:

**Theorem 4.9.** *Under Assumptions 2.1 and 3.1 with $H \geq 4d H_0$ the error in the approximate solution $\mathbf{u}_H^k$, defined in Eq. (18), fulfills*

$$|\mathbf{u} - \mathbf{u}_H^k|_{\mathbf{K}} \leq C_{\alpha,\beta,d,\mu,\sigma} k^{d/2} \left(H + \exp(-k(6C_1C_2)^{-1})\right) |\mathbf{f}|_{\mathbf{M}^{-1}}.$$

**Proof.** By Galerkin orthogonality $|\mathbf{u} - \mathbf{u}_H^k|_{\mathbf{K}} \leq |\mathbf{u} - \mathbf{v}|_{\mathbf{K}}$ for all $\mathbf{v} \in \mathbf{V}_H^{\mathrm{ms},k}$. We let $\mathbf{v} = (1 - \mathbf{Q}^k)\mathcal{I}\mathbf{u}_H \in \mathbf{V}_H^{\mathrm{ms},k}$ and use the identity $\mathbf{u}_H = (1 - \mathbf{Q})\mathcal{I}\mathbf{u}_H$. Using the triangle inequality we therefore have

$$|\mathbf{u} - \mathbf{u}_H^k|_{\mathbf{K}} \leq |\mathbf{u} - \mathbf{u}_H|_{\mathbf{K}} + |(\mathbf{Q} - \mathbf{Q}^k)\mathcal{I}\mathbf{u}_H|_{\mathbf{K}}.$$

The first part is treated in Lemma 4.2. For the second part we use the triangle inequality, Lemma 4.8, and that $\mathbf{L}$ and therefore $\mathbf{K}$ is stable with respect to $\mathcal{I}$ in the $\mathbf{K}$ norm

$$\begin{aligned} |(\mathbf{Q} - \mathbf{Q}^k)\mathcal{I}\mathbf{u}_H|_{\mathbf{K}}^2 &\leq C_{\alpha,\beta,d,\mu,\sigma} k^d \exp(-k(3C_1C_2)^{-1})|\mathcal{I}\mathbf{u}_H|_{\mathbf{K}}^2 \\ &\leq C_{\alpha,\beta,d,\mu,\sigma} k^d \exp(-k(3C_1C_2)^{-1})|\mathbf{u}_H|_{\mathbf{K}}^2 \\ &\leq C_{\alpha,\beta,d,\mu,\sigma} k^d \exp(-k(3C_1C_2)^{-1})|\mathbf{f}|_{\mathbf{M}^{-1}}^2. \end{aligned}$$

where we use the equivalence of the $\mathbf{K}$ and $\mathbf{L}$ norms and that $|\mathbf{u}_H|_{\mathbf{K}} \leq |\mathbf{u}|_{\mathbf{K}} \leq C_\alpha |\mathbf{f}|_{\mathbf{M}^{-1}}$. The theorem follows. $\square$

## 5. Numerical examples

We first consider a scalar example modeling heat conduction and then we turn to a structural problem where we seek the displacement of a fiber network. For all numerical examples, we use the network shown in Fig. 8. Uniformly rotated line segments of length 0.05 are uniformly distributed in the unit square so that the total mass is $|1|_M^2 = 1000$, resulting in about 20 000 line segments. The line segments are discretized with nodes and edges. All cross points are in particular represented by nodes. The total number of nodes in the generated network is around 80 000.

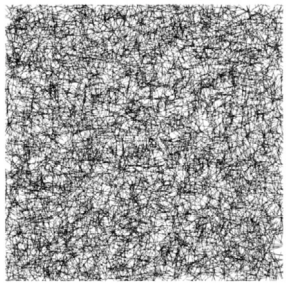

**Fig. 8.** The network analyzed in the numerical examples. It is constructed by around 20 000 line segments of length 0.05 uniformly distributed in the unit square. Crossings of line segments are represented by nodes.

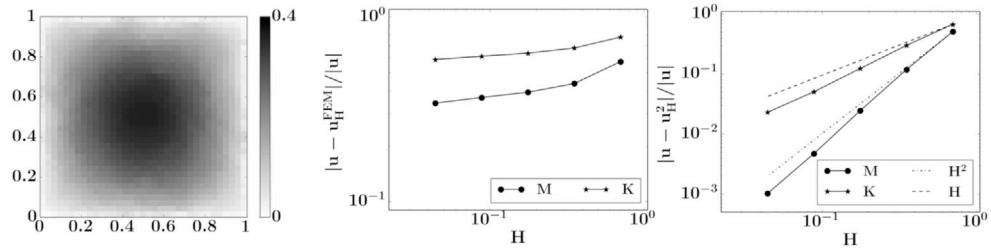


**Fig. 9.** The solution $u$ to the problem in Section 5.1, along with the convergence results for a finite element approach and the LOD method with localization factor $k = 2$.

### 5.1. Heat conduction

We consider the model problem introduced in Example 2.2 for the two-dimensional network in Fig. 8 and adopt the scalar notation from Example 2.2. The solution represents temperature (scalar) in each node, and the node-wise operator, $K_x$, is defined as:

$$(K_x v, w) = \frac{1}{2} \sum_{y \sim x} \gamma_{xy} \frac{(v(x) - v(y))(w(x) - w(y))}{|x - y|},$$

where the coefficients $\gamma_{xy} \in [0.1, 1]$ are chosen at random for each edge $\{x, y\}$. The computational domain is the unit square $\Omega = [0, 1]^2$. The problem considered has a constant right hand side weighted with the mass matrix $M$ and zero Dirichlet boundary is applied on the entire boundary, i.e.

$$\begin{cases} Ku = f, \\ u(\partial\Omega) = 0, \end{cases}$$

with $K = \sum_{x \in \mathcal{N}} K_x$, $f = M1$ and $1 \in \hat{V}$. The exact solution is compared to the LOD approximation 4.3 with localization parameter $k = 2$ for different coarse grids. To show that the problem cannot easily be solved using the coarse finite element spaces $V_H$ we also consider the problem:

$$\text{find } u_H^{\text{FEM}} \in V_H \ : \ (Ku_H^{\text{FEM}}, v) = (M1, v) \text{ for all } v \in V_H. \tag{23}$$

An illustration of the solution, $u$, and the errors of the direct finite element approach and the LOD approximations in both $K$ and $M$ norm are presented in Fig. 9. The results show a convergence plateau for the finite element approach, whereas the theoretical convergence rate of $H$ (Theorem 4.9) is achieved for the LOD method already for a localization parameter of $k = 2$. Moreover, we observe that error is proportional to $H^2$ in the $M$-norm for the LOD method.

### 5.2. A fiber network model

Here two variations of Example 2.4 are considered. The network in Fig. 8 should be interpreted as a mesh of round steel wires of radius $r_w = 2.5 \times 10^{-3}$. Eq. (7) is a linearized version of Hooke's law with parameter $\gamma_{xy} = \gamma_1 = EA$, where $A = \pi r_w^2$ is the cross-section area of the wire and $E = 210\,\text{GPa}$ its Young's modulus. The bending forces are handled by adding the equations in (8). These additions are linearized versions of Euler–Bernoulli with parameters $\gamma_{xyz} = 2EI(|x - y| + |x - z|)^{-2}$ where $E$ is the same Young's modulus and $I = 0.25\pi r_w^4 = 0.25 A r_w^2$ is the second moment of area of the wire. The two coefficients are related in the following way,

$$\gamma_{xyz} = EA \frac{r_w^2}{2(|x - y| + |x - z|)^2} = \gamma_1 \frac{r_w^2}{2(|x - y| + |x - z|)^2},$$

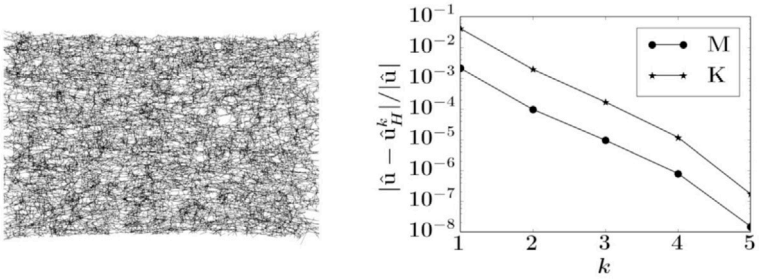


**Fig. 10.** The solution of the strained fiber network along with the normalized approximation errors for different localization parameter $k$.

where $0.05 \leq \frac{r_w}{|x-y|} \leq 5$ for any edge $x \sim y$. This relation is dependent on the lengths of the edges, where the edge lengths in turn depend on how the fibers intersect each other. Because of this $\gamma_{xyz}$ varies rapidly in space.

*Pure displacement problem*

The first structural problem we consider is a tensile simulation, where one side of the unit square is fixed, and the opposite side is displaced. This displacement stretches the network, and the solution to the problem is the equilibrium of the network given the displacement. We will only consider forces and displacements in the plane the network resides in for this simulation, meaning that any $x_3$-directional components are left out. The problem can be written as

$$\begin{cases} \mathbf{K}\hat{\mathbf{u}} = \mathbf{0}, \\ \hat{\mathbf{u}}(\Gamma_1) = [0,0]^T, \ \hat{\mathbf{u}}(\Gamma_2) = [0.5,0]^T, \end{cases}$$

where $\Gamma_1$ is any point with x-coordinate 0, and $\Gamma_2$ is any point with $x$-coordinate 1. The solution is presented in Fig. 10. Solving this problem with the LOD method requires some extra steps compared to the previous example as we have non-vanishing Dirichlet conditions. As mentioned in Section 2.3, we introduce an auxiliary function, $\mathbf{g}$, such that $\hat{\mathbf{u}} = \mathbf{u} + \mathbf{g}$ and consider,

$$\begin{cases} \mathbf{K}\mathbf{u} = -\mathbf{K}\mathbf{g}, \\ \mathbf{u}(\Gamma_1 \cup \Gamma_2) = [0,0]^T. \end{cases}$$

For this specific problem we choose $\mathbf{g}(x) = [0.5x_1, 0]^T$ which is in $\hat{\mathbf{V}}_H$ for all $H$. It was shown in [2] that if $\mathbf{g} \in \hat{\mathbf{V}}_H$ then the exact solution of this support problem can be written as $\mathbf{u} = \mathbf{u}_H + \mathbf{c}_H$, where $\mathbf{c}_H$ is attainable with an extended version of $\mathbf{Q}$. This is seen by first writing the corrector term, $\mathbf{c}_H$, as the solution to the following variational problem:

$$\text{find } \mathbf{c}_H \in \mathbf{W} \ : \ (\mathbf{K}\mathbf{c}_H, \mathbf{w}) = (\mathbf{K}(-\mathbf{g}), \mathbf{w}) \text{ for all } \mathbf{w} \in \mathbf{W},$$

by using that $\mathbf{V} = \mathbf{V}^{\text{ms}} \bigoplus \mathbf{W}$, $\mathbf{V}^{\text{ms}} \perp_{\mathbf{K}} \mathbf{W}$, and $\mathbf{K}$ being coercive. The solution to this variational problem can be written as $\hat{\mathbf{Q}}(-\mathbf{g})$, where $\hat{\mathbf{Q}} : \hat{\mathbf{V}} \to \mathbf{W}$ is the extended projection operator of $\mathbf{Q}$:

$$(\mathbf{K}\hat{\mathbf{Q}}\mathbf{v}, \mathbf{w}) = (\mathbf{K}\mathbf{v}, \mathbf{w}) \text{ for all } \mathbf{w} \in \mathbf{W}.$$

With $\hat{\mathbf{Q}}_T$ and $\hat{\mathbf{Q}}_T^k$ derived analogously to $\mathbf{Q}_T$ and $\mathbf{Q}_T^k$. In practice, finding this extension, $\hat{\mathbf{Q}}$, is comparable to finding $\mathbf{Q}$ in terms of computational complexity. Using this projection operator we can write the exact solution to the initial problem as:

$$\hat{\mathbf{u}} = \mathbf{u} + \mathbf{g} = \mathbf{u}_H + \mathbf{c}_H + \mathbf{g} = \mathbf{u}_H + (1 - \hat{\mathbf{Q}})\mathbf{g},$$

and the localized LOD approximations:

$$\hat{\mathbf{u}}_H^k = \mathbf{u}_H^k + (1 - \hat{\mathbf{Q}}^k)\mathbf{g}.$$

For an extended discussion on how to handle general Dirichlet data in the LOD method, see [20].

In the numerical experiment, the exponential decay of the correctors are analyzed, by fixing $H = 1/32$ and computing the errors $|\hat{\mathbf{u}}_H^k - \hat{\mathbf{u}}|$ for different $k$. The results are presented in Fig. 10, and exponential decay is observed in both the $\mathbf{K}$ and $\mathbf{M}$ norm which is consistent with Theorem 4.9.

*Displacement problem with lateral load*

In the second numerical example of the fiber network problem, we introduce a lateral ($x_3$-directional) load to the previous tensile problem. This problem can be expressed as the following linear system:

$$\begin{cases} \mathbf{K}\hat{\mathbf{u}} = \mathbf{f}, \\ \hat{\mathbf{u}}(\Gamma_1) = [0,0,0]^T, \ \hat{\mathbf{u}}(\Gamma_2) = [0.5,0,0]^T, \end{cases}$$

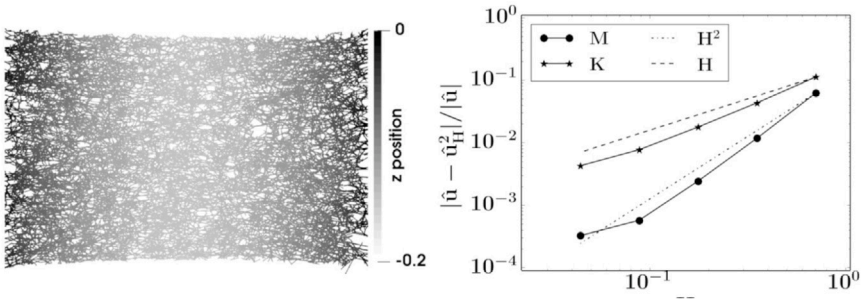


**Fig. 11.** Illustration of the solution (XY-plane) and the normalized errors of the LOD approximations $\hat{\mathbf{u}}_H^2$ for varying $H$.

where $\Gamma_1$ is any point with x-coordinate 0, $\Gamma_2$ any point with x-coordinate 1, and $\mathbf{f} = \mathbf{Mh}$ with $\mathbf{h}$ as the constant function $[0, 0, -10^5]$. As with the previous example, we let $\mathbf{g}(x) = [0.5x_1, 0, 0]^T \in \hat{\mathbf{V}}_H$ and

$$\begin{cases} \mathbf{Ku} = \mathbf{f} - \mathbf{Kg}, \\ \mathbf{u}(\Gamma_1 \cup \Gamma_2) = [0, 0, 0]^T \end{cases}$$

where $\hat{\mathbf{u}} = \mathbf{u} + \mathbf{g}$. Using the same motivation as in the previous example, the localized LOD approximations considered are:

$$\hat{\mathbf{u}}_H^k = \mathbf{u}_H^k + (1 - \hat{\mathbf{Q}}^k)\mathbf{g}.$$

However, unlike the previous example we cannot guarantee that the ideal LOD approximation, $\hat{\mathbf{u}}_H$, is the exact solution $\hat{\mathbf{u}}$, since $\mathbf{f} \neq \mathbf{0}$. Theorem 4.9 is numerically confirmed, with localization parameter $k = 2$, and presented in Fig. 11, along with the reference solution $\hat{\mathbf{u}}$. The $H$ convergence is seen in the $\mathbf{K}$-norm as the theory indicates, but some slight stagnation is observed for the finest grid considered which would vanish for $k = 3$ as indicated in Fig. 10. Already for $k = 2$ the method produces highly accurate results in both $\mathbf{K}$ and $\mathbf{M}$ norm, with less than one percent relative error in the $\mathbf{K}$ norm and a tenth of a percent in the $\mathbf{M}$ norm for the finest coarse grid considered.

## Declaration of competing interest

The authors declare the following financial interests/personal relationships which may be considered as potential competing interests: Morgan Görtz reports financial support was provided by the Swedish Foundation for Strategic Research. Axel Målqvist reports financial support was provided by the Göran Gustafsson Foundation for Research in Natural Sciences and Medicine and by the Swedish Research Council. Fredrik Hellman reports financial support was provided by the Göran Gustafsson Foundation for Research in Natural Sciences and Medicine. Gustav Kettil reports financial support was provided by the Swedish Research Council and the Åforsk Foundation.

## Data availability

The authors do not have permission to share data.

## Acknowledgments

The Swedish Foundation for Strategic Research (SSF), Sweden supports the second author, the third and fifth author are supported by the Göran Gustafsson Foundation for Research in Natural Sciences and Medicine, Sweden, the fourth author was funded by The Åforsk Foundation, Sweden research grant 22-166: "Development of simulation tools for bending and fracture propagation of fiber based materials", and the Swedish Research Council, Sweden supports the fourth and fifth author in project number 2019-03517 VR. The computations were enabled by resources provided by Chalmers e-Commons at Chalmers.

## Appendix. The technical proofs

**Proof of Lemma 3.4.** Since the basis functions $\varphi_k$ have a Lipschitz constant $H^{-1}$ we have

$$|\varphi_k|_{L,S}^2 = \sum_{x \in \mathcal{N}(S)} (L_x \varphi_k, \varphi_k) = \frac{1}{2} \sum_{x \in \mathcal{N}(S)} \sum_{x \sim y} \frac{(\varphi_k(x) - \varphi_k(y))^2}{|x - y|} \leq H^{-2} |1|_{M,S}^2 \tag{24}$$

and therefore, since $0 \leq \varphi_k \leq 1$,

$$|\varphi_k|_{M,S} + H|\varphi_k|_{L,S} \leq 2|1|_{M,S}. \tag{25}$$

We turn to the dual basis $\psi_k$. To relieve the notation, we omit subscript $k$ and set $\psi = \psi_k$ and $T = T_k$ in this proof. Denote the mesh vertices in $T$ by $y_1, \dots, y_{2^d}$ and let $y_1$ be the vertex for which $\psi$ is the dual basis. We define the positive semi-definite Gram matrix $\Lambda$ with entries $\Lambda_{ij} = (M_T\varphi_j, \varphi_i)$ for $i, j = 1, \dots, 2^d$. Let $\alpha = (\alpha_1, \dots, \alpha_{2^d})^T$ and express the dual basis as $\psi = \sum_{\ell=1}^{2^d} \alpha_\ell \varphi_\ell$. Then by the definition of $\psi$, we have $\alpha = \Lambda^{-1}(1, 0, \dots, 0)^T$ and that the sought squared norm $(M_T\psi, \psi) = \alpha_1 \le \lambda_1(\Lambda)^{-1}$, where $\lambda_1(\Lambda)$ is the smallest eigenvalue of $\Lambda$. To be able to bound this eigenvalue from below, we split $\Lambda$ into the significant contributions from network nodes close to the corners of the element.

Let $\hat{T}_\ell = \{x \in T : y_\ell + (x - y_\ell)/r \in \overline{T}\}$ be the points in $T$ that is in an $r$ scaling of $\overline{T}$ in the corner of node $y_\ell$. We set $r = 1/(4d)$, but keep writing $r$ for brevity. Since the closure of $\hat{T}_\ell$ is a scaling of $\overline{T}$, it is a hypercube of side length $rH \ge H_0$. We set $\hat{T}_0 = T \setminus \hat{T}_1 \setminus \cdots \setminus \hat{T}_\ell$ and define the symmetric positive semi-definite matrices $\Lambda^\ell$ for $\ell = 0, 1, \dots, 2^d$ with entries $\Lambda^\ell_{ij} = (M_{\hat{T}_\ell}\varphi_j, \varphi_i)$. We can then write $\Lambda = \Lambda^0 + \Lambda^1 + \cdots + \Lambda^{2^d}$. Since $x \mapsto \varphi_j(x)\varphi_i(x)$ is continuous and $\hat{T}_\ell$ is path-connected, by the intermediate value theorem there is an $x_\ell \in \hat{T}_\ell$ such that

$$\Lambda^\ell_{ij} = (M_{\hat{T}_\ell}\varphi_j, \varphi_i) = \sum_{x \in \mathcal{N}(\hat{T}_\ell)} |1|^2_{M,\{x\}} \varphi_i(x)\varphi_j(x) = |1|^2_{M,\hat{T}_\ell} \varphi_i(x_\ell)\varphi_j(x_\ell).$$

Using the properties of the smallest eigenvalues of symmetric real operators $A$ and $B$: (i) $\lambda_1(A + B) \ge \lambda_1(A) + \lambda_1(B)$ and (ii) $\lambda_1(\alpha A + \beta B) \ge \min(\alpha, \beta)\lambda_1(A + B)$, we get

$$\lambda_1(\Lambda) \ge \lambda_1(\Lambda^0) + \lambda_1(\Lambda^1 + \cdots + \Lambda^{2^d}) \ge \lambda_1(\Lambda^1 + \cdots + \Lambda^{2^d}) \ge \min_\ell |1|^2_{M,\hat{T}_\ell} \lambda_1(G)$$

where $G$ is a matrix with entries $G_{ij} = \sum_{\ell=1}^{2^d} \varphi_i(x_\ell)\varphi_j(x_\ell)$. The next step is to bound $\lambda_1(G)$ from below by means of the Gershgorin circle theorem.

We study the first row of $G$ and note that all entries in the row are positive. The distance $D_1$ between zero and the Gershgorin disc for the first row can be expressed as the difference between the diagonal entry and the sum of the (all positive) non-diagonal entries on the row, i.e.

$$\begin{aligned} D_1 &= G_{11} - \sum_{\ell=2}^{2^d} G_{1\ell} = \sum_{\ell=1}^{2^d} \varphi_1(x_\ell)^2 - \varphi_1(x_\ell) \sum_{j=2}^{2^d} \varphi_j(x_\ell) \\ &= \sum_{\ell=1}^{2^d} \varphi_1(x_\ell)(2\varphi_1(x_\ell) - 1) = \varphi_1(x_1)(2\varphi_1(x_1) - 1) + \sum_{\ell=2}^{2^d} \varphi_1(x_\ell)(2\varphi_1(x_\ell) - 1), \end{aligned}$$

where the partition of unit of the basis functions was used. Since $x_\ell \in \hat{T}_\ell$, the values of the basis function $\varphi_1$ in these points are bounded as follows

$$\begin{aligned} (1 - r)^d \le \varphi_1(x_1) \le 1 \quad &\text{and} \\ 0 \le \varphi_1(x_\ell) \le r^k \quad &\text{if } y_1 \text{ and } y_\ell \text{ differ in } 1 \le k \le d \text{ components.} \end{aligned}$$

The condition for the second bound can also be phrased as $k$ being the minimum number of edges of the hypercube $T_\ell$ to traverse to reach $y_\ell$ from $y_1$. We note that, for each $k$, there are $\binom{d}{k}$ element corners $y_\ell$ for which this condition hold. This allows us to write

$$\sum_{\ell=2}^{2^d} \varphi_1(x_\ell) \le \sum_{k=1}^{d} \binom{d}{k} r^k = (1 + r)^d - 1,$$

which will be useful next.

With the particular choice $r = 1/(4d)$, we use Bernoulli's inequality $(1-r)^d \ge 1 - rd = 3/4$ to bound $2\varphi_1(x_1) - 1 \ge 2(1-r)^d - 1 \ge 1/2$. Using this inequality again, together with $2\varphi_1(x_\ell) - 1 \ge -1$ and $(1 + r)^d \le e^{rd} = e^{1/4}$, we bound $D_1$ as follows,

$$D_1 \ge \frac{1}{2}\varphi_1(x_1) - \sum_{\ell=2}^{2^d} \varphi_1(x_\ell) \ge \frac{1}{2}(1 - r)^d - (1 + r)^d + 1 \ge \frac{3}{8} - e^{1/4} + 1 > 0.$$

Thus, the distance between zero and the Gershgorin disc for the first row is bounded below by a positive constant. The argument can be repeated for the $2^d$ rows and we get that all eigenvalues of $G$ are bounded below, and in particular that $\lambda_1(G) \ge C$. We obtain the asserted inequality

$$|\psi|^2_{M,T} = (M_T\psi, \psi) \le \lambda_1(\Lambda)^{-1} \le (4d)^d \max_\ell |1|^{-2}_{M,\hat{T}_\ell} \lambda_1(G)^{-1} \le C_d \max_\ell |1|^{-2}_{M,\hat{T}_\ell}.$$

Altogether, using Assumption 3.1.1, and Eq. (25) we conclude

$$\left(|\varphi_k|_{M,S} + H|\varphi_k|_{L,S}\right) |\psi_k|_{M,T_k} \le C_d \sigma^{1/2} \tag{26}$$

for any $S \in \mathcal{T}_H$. □

**Proof of Lemma 4.5.** We start with the first inequality. Pick a $T \in \mathcal{T}_H$. Since $\mathbf{w}_j \in \mathbf{V}(U_2(y_j))$ and $\mathbf{K}_T\mathbf{v} = 0$ for $\mathbf{v} \in \mathbf{V}(\Omega \setminus U(T))$, we have that $\mathbf{K}_T\mathbf{w}_j$ can be non-zero for at most $C_d$ mesh nodes $j$, where $C_d$ depends only on $d$. Since $\mathbf{K}_T$ is locally defined in this sense, we get

$$|\mathbf{w}|^2_{\mathbf{K},T} \le C_d \sum_{j=1}^{m} |\mathbf{w}_j|^2_{\mathbf{K},T}.$$

Summation over $T \in \mathcal{T}_H$ proves the inequality with $C_2 = C_d$.

For the second inequality we first consider the $\mathbf{L}$-norm. We use Lemma 3.5 componentwise and globally, inequality (20), the fact that $\mathcal{I}\mathbf{w} = 0$, Lemma 3.5 again, and finally a similar locality argument of $\mathbf{L}_T$ as in the previous paragraph and get

$$\begin{aligned}\sum_{j=1}^{m} |\mathbf{w}_j|^2_{\mathbf{L}} &\le C_{d,\mu,\sigma} \sum_{j=1}^{m} |\varphi_j \mathbf{w}|^2_{\mathbf{L}} \\ &\le C_{d,\mu,\sigma} \sum_{j=1}^{m} \sum_{T\in\mathcal{T}_H} \left( H^{-2}|\mathbf{w}|^2_{\mathbf{M},T} + |\mathbf{w}|^2_{\mathbf{L},T} \right) \\ &\le C_{d,\mu,\sigma} \sum_{j=1}^{m} \sum_{T\in\mathcal{T}_H} |\mathbf{w}|^2_{\mathbf{L},U_3(T)} \\ &\le C_{d,\mu,\sigma} |\mathbf{w}|^2_{\mathbf{L}}.\end{aligned}$$

We use equivalence of $\mathbf{L}$- and $\mathbf{K}$-norms to get the second inequality with $C_1 = C_{\alpha,\beta,d,\mu,\sigma}$. □

**Proof of Lemma 4.8.** We use $\mathbf{R}^{\ell}_T$ as an intermediate step to show that

$$\begin{aligned}|\mathbf{Q}_T\mathbf{v}|_{\mathbf{L},\Omega\setminus U_{3\ell+1}(T)} &\le |\mathbf{Q}_T\mathbf{v} - \mathbf{R}^{\ell}_T\mathbf{v}|_{\mathbf{L}} + |\mathbf{R}^{\ell}_T\mathbf{v}|_{\mathbf{L},\Omega\setminus U_{3\ell+1}(T)} \\ &\le \alpha^{-1/2}|\mathbf{Q}_T\mathbf{v} - \mathbf{R}^{\ell}_T\mathbf{v}|_{\mathbf{K}} + |\mathbf{R}^{\ell}_T\mathbf{v}|_{\mathbf{L},\Omega\setminus U_{3\ell+1}(T)} \\ &\le \alpha^{-1/2}\exp(-\ell(2C_1C_2)^{-1})|\mathbf{v}|_{\mathbf{K},T}.\end{aligned} \tag{27}$$

The term $|\mathbf{R}^{\ell}_T\mathbf{v}|_{\mathbf{L},\Omega\setminus U_{3\ell+1}(T)}$ is zero since by Eq. (19) $\mathbf{R}^{\ell}_T\mathbf{v}$ is zero outside $U_{3\ell}(T)$ and $\mathbf{L}$ only spreads information one layer.

We let $\eta \in V_H$ be a cut-off function such that $(1-\eta)(x_i) = 0$ for all $x_i \in U_{k-2}(T)$ and $(1-\mathcal{I})(\eta\mathbf{Q}_T\mathbf{v}) \in \mathbf{W}(U_k(T))$. Since $\mathbf{Q}^k_T\mathbf{v}$ is the best approximation of $\mathbf{Q}_T\mathbf{v}$ in $\mathbf{W}(U_k(T))$ we get

$$\begin{aligned}|\mathbf{Q}_T\mathbf{v} - \mathbf{Q}^k_T\mathbf{v}|^2_{\mathbf{K}} &\le |\mathbf{Q}_T\mathbf{v} - (1-\mathcal{I})(\eta\mathbf{Q}_T\mathbf{v})|^2_{\mathbf{K}} = |(1-\mathcal{I})(\mathbf{Q}_T\mathbf{v} - \eta\mathbf{Q}_T\mathbf{v})|^2_{\mathbf{K}} \\ &\le \beta|(1-\mathcal{I})(\mathbf{Q}_T\mathbf{v} - \eta\mathbf{Q}_T\mathbf{v})|^2_{\mathbf{L}} \le C_{\beta,d,\mu,\sigma}|(1-\eta)\mathbf{Q}_T\mathbf{v}|^2_{\mathbf{L}}\end{aligned}$$

using the equivalence of the $\mathbf{L}$ and $\mathbf{K}$ norms and Lemma 3.5. Next we use the inequality (20), since $\eta \in V_H$, and Lemma 3.5 to get

$$\begin{aligned}|(1-\eta)\mathbf{Q}_T\mathbf{v}|^2_{\mathbf{L}} &= \sum_{T'\in\mathcal{T}_H} |(1-\eta)\mathbf{Q}_T\mathbf{v}|^2_{\mathbf{L},T'} \\ &= \sum_{T'\in\mathcal{T}_H} |(1-\eta)\mathbf{Q}_T\mathbf{v}|^2_{\mathbf{L},T'\cap\Omega\setminus U_{k-3}(T)} \\ &\le 2\sum_{T'\in\mathcal{T}_H} H^{-2}|\mathbf{Q}_T\mathbf{v}|^2_{\mathbf{M},T'\cap\Omega\setminus U_{k-3}(T)} + |\mathbf{Q}_T\mathbf{v}|^2_{\mathbf{L},T'\cap\Omega\setminus U_{k-3}(T)} \\ &\le 2\sum_{T'\in\mathcal{T}_H} H^{-2}|(1-\mathcal{I})\mathbf{Q}_T\mathbf{v}|^2_{\mathbf{M},T'\cap\Omega\setminus U_{k-3}(T)} + |\mathbf{Q}_T\mathbf{v}|^2_{\mathbf{L},T'\cap\Omega\setminus U_{k-3}(T)} \\ &\le C_{d,\mu,\sigma}\sum_{T'\in\mathcal{T}_H} |\mathbf{Q}_T\mathbf{v}|^2_{\mathbf{L},T'\cap\Omega\setminus U_{k-6}(T)} \\ &= C_{d,\mu,\sigma}|\mathbf{Q}_T\mathbf{v}|^2_{\mathbf{L},\Omega\setminus U_{k-6}(T)}.\end{aligned}$$

We use Eq. (27) with $\ell = k/3 - 7/3$ to conclude

$$|\mathbf{Q}_T\mathbf{v} - \mathbf{Q}^k_T\mathbf{v}|_{\mathbf{K}} \le C_{\alpha,\beta,d,\mu,\sigma}\exp(-k(6C_1C_2)^{-1})|\mathbf{v}|_{\mathbf{K},T}. \tag{28}$$

Next we follow the proof of Theorem 4.3 in [9]. Let $\eta \in V_H$ be 1 for $x \in \Omega \setminus U_{k+3}(T)$ and 0 for all $x \in U_{k+2}(T)$. We let $\mathbf{e} = (\mathbf{Q} - \mathbf{Q}^k)\mathbf{v}$ and $\mathbf{e}_T = (1-\mathcal{I})(\eta\mathbf{e}) \in \mathbf{W}$ with $\mathbf{e}_T(x) = 0$ for all $x \in U_{k+1}(T)$. We note that

$$(\mathbf{K}\mathbf{e}_T, \mathbf{e}) = (\mathbf{K}\mathbf{e}_T, \mathbf{Q}_T\mathbf{v}) = (\mathbf{K}_T\mathbf{e}_T, \mathbf{v}) = 0$$

since $\mathbf{Q}^k_T\mathbf{v}(x) = 0$ for all $x \in \Omega \setminus U_k(T)$ and $\mathbf{K}\mathbf{e}_T(x) = 0$ for all $x \in U_k(T)$ and that $\mathbf{K}_T\mathbf{e}_T = 0$. We have $\mathbf{e} - \mathbf{e}_T = (1-\eta)\mathbf{e} + \mathcal{I}(\eta\mathbf{e}) = (1-\mathcal{I})((1-\eta)\mathbf{e}) \in \mathbf{W}(U_{k+4}(T))$. We conclude, using Eq. (28),

$$\begin{aligned}|\mathbf{e}|^2_{\mathbf{K}} &= \sum_{T\in\mathcal{T}_H} (\mathbf{K}(1-\mathcal{I})((1-\eta)\mathbf{e}), (\mathbf{Q}_T - \mathbf{Q}^k_T)\mathbf{v}) \\ &\le C_{\alpha,\beta,d,\mu,\sigma}\exp(-k(6C_1C_2)^{-1}) \sum_{T\in\mathcal{T}_H} |\mathbf{e}|_{\mathbf{K},U_{k+5}(T)}|\mathbf{v}|_{\mathbf{K},T} \\ &\le C_{\alpha,\beta,d,\mu,\sigma}k^{d/2}\exp(-k(6C_1C_2)^{-1})|\mathbf{e}|_{\mathbf{K}}|\mathbf{v}|_{\mathbf{K}}\end{aligned}$$

where we use that one element $T$ is only covered by a finite number of patches $U_{k+5}(T)$. The lemma follows after division by $|\mathbf{e}|_{\mathbf{K}}$. □

## References


[1] J. Chu, B. Engquist, M. Prodanović, R. Tsai, A multiscale method coupling network and continuum models in porous media I: steady-state single phase flow, Multiscale Model. Simul. 10 (2012) 515–549.
[2] G. Kettil, A. Målqvist, A. Mark, M. Fredlund, K. Wester, F. Edelvik, Numerical upscaling of discrete network models, BIT 60 (2020) 67–92.
[3] E. Svenning, A. Mark, F. Edelvik, E. Glatt, S. Rief, A. Wiegmann, L. Martinsson, R. Lai, M. Fredlund, U. Nyman, Multiphase simulation of fiber suspension flows using immersed boundary methods, Nord. Pulp Pap. Res. J. 27 (2) (2012) 184–191.
[4] A. Brandt, Multi-level adaptive solutions to boundary-value problems, Math. Comp. 31 (1977) 333–390.
[5] R. Kornhuber, H. Yserentant, Numerical homogenization of elliptic multiscale problems by subspace decomposition, Multiscale Model. Simul. 14 (3) (2016) 1017–1036.
[6] Y. Efendiev, J. Galvis, T.Y. Hou, Generalized multiscale finite element methods (gmsfem), J. Comput. Phys. 251 (2013) 116–135.
[7] H. Owhadi, C. Scovel, Operator-Adapted Wavelets, Fast Solvers, and Numerical Homogenization, in: Cambridge Monographs on Applied and Computational Mathematics, vol. 35, Cambridge University Press, Cambridge, UK, 2019.
[8] A. Må lqvist, D. Peterseim, Localization of elliptic multiscale problems, Math. Comp. 83 (2014) 2583–2603.
[9] A. Målqvist, D. Peterseim, Numerical Homogenization By Localized Orthogonal Decomposition, SIAM Spotlights, ISBN: 978-1-611976-44-1, 2020.
[10] R. Ewing, O. Iliev, R. Lazarov, I. Rybak, J. Willems, A simplified method for upscaling composite materials with high contrast of the conductivity, SIAM J. Sci. Comput. 31 (2009) 2568–2586.
[11] O. Iliev, R. Lazarov, J. Willems, Fast numerical upscaling of heat equation for fibrous materials, Comput. Vis. Sci. 13 (2010) 275–285.
[12] J. Bishop, J. Emery, Field R., C. Weinberger, D. Littlewood, Direct numerical simulations in solid mechanics for understanding the macroscale effects of microscale material variability, Comput. Methods Appl. Mech. Eng. 287 (2015) 262–289.
[13] X. Yin, W. Chen, A. To, C. McVeigh, W. Kam Liu, Statistical volume element method for predicting microstructure–constitutive property relations, Comput. Methods Appl. Mech. Eng., 197 (43-44) 3516–3529.
[14] R. Mansour, A. Kulachenko, 4 - stochastic constitutive model of thin fibre networks, in: Mechanics of Fibrous Networks, in: Elsevier Series in Mechanics of Advanced Materials, Elsevier, 2022, pp. 75–112.
[15] F. Della Rossa, C. D'Angelo, F. Quarteroni, A distributed model of traffic flows on extended regions, Netw. Heterog. Media 5 (2010) 525–544.
[16] M. Görtz, F. Hellman, A. Målqvist, Iterative solution of spatial network models by subspace decomposition, Math. Comp. 93 (2024) 233–258.
[17] R. Scott, S. Zhang, Finite element interpolation of nonsmooth functions satisfying boundary conditions, Math. Comp. 54 (1990) 483–493.
[18] F. Hellman, A. Målqvist, Numerical homogenization of elliptic PDEs with similar coefficients, Multimedia Model. Simul. 17 (2019) 650–674.
[19] R. Kornhuber, D. Peterseim, H. Yserentant, An analysis of a class of variational multiscale methods based on subspace decomposition, Math. Comp. 87 (314) (2018) 2765–2774.
[20] P. Henning, A. Målqvist, Localized orthogonal decomposition techniques for boundary value problems, SIAM J. Sci. Comput. 36 (2014) A1609–A1634.